Exploring Oxygen Delivery Strategies for Oxidative Coupling of Methane

Undergraduate Research Thesis in Chemical Engineering

Presented in Partial Fulfillment of the Requirements for Graduation with Research Distinction from the Department of Chemical and Biomolecular Engineering at The Ohio State University

By

Michael A. Jindra

The Ohio State University

April 2017

Thesis Committee:

Dr. Liang-Shih Fan, Advisor

Dr. Lisa Hall

Abstract

A myriad of metal oxide catalysts have been explored for upgrading methane into higher hydrocarbons in a process called oxidative coupling of methane (OCM). Because of the ramifications of utilizing methane as a chemical feedstock, efforts to optimize the reactor design and catalyst for OCM process have been ongoing since 1980. Catalytic oxygen carriers (COCs) used for cycling oxygen to the reactant gas in OCM reaction processes have shown distinct advantages over cofeeding reaction schemes. Manganese based COCs have exhibited multiple oxidation states that function in the cyclic reduction-oxidation reactions of OCM. This study aims to elucidate the different forms of oxygen delivery strategies that can be leveraged from a deeper understanding of how these COC oxidation states effect product distributions. The COC particles used to facilitate this oxygen transfer in this study were Mg_6MnO_8 and $Li_{0.2}Mg_{5.8}MnO_8$. Thermogravimetric analysis and fixed bed experiments were performed to characterize the effects of the Mn^{4+} and Mn^{3+} oxidation states on methane conversion and C_{2+} selectivity. The Mn^{4+} oxidation state was shown to experience higher reduction rates, higher conversion, and lower selectivity than the Mn^{3+} oxidation state. Li doping of the manganese oxide was shown to reduce reduction rates, lowering conversion and raising selectivity. This study showed that reduction rate and ultimately product distribution can be tuned by adjusting the oxidation state of manganese based COCs.

For Alessa

Acknowledgments

I cannot begin this work without first thanking Professor Liang-Shih Fan for the tremendous opportunity to be a member of his research team. I owe much of the success of my early career to the mentorship and training I have received while an undergraduate researcher at Ohio State University. With my whole heart I am grateful to Elena Chung for inviting me to join this team of brilliant researchers and for continuing to be an invaluable mentor and dear friend. I am grateful for Hussein Alkhatib, Mandar Kathe, and Sourabh Nadgouda for introducing me to exceptional academic research and the community of researchers at Ohio State. Sourabh has been a phenomenal teacher and listener, and I hope that more undergraduates have the privilege to learn from him. Last and not least, I am deeply grateful to Deven Baser for his strong leadership in the chemical looping team and involvement in this work. I hope that I can attempt to return the value that Deven has contributed to my development through this thesis.

Vita

2012.....Padua Franciscan High School, Parma, OH

2012 to present .....B.S. Chemical Engineering, The Ohio State University

Publications

Thompson, V.S., Lacey, J.A., Hartley, D.S., **Jindra, M.A.**, Aston, J.E., Thompson, D.N. (2015). Application of air classification and formulation to manage feedstock cost, quality and availability for bioenergy. *Fuel*, 180-505. April 2016.

Chung, E.Y., Wang, W.K., Alkhatib, H., Nadgouda, S., **Jindra, M.A.**, Sofranko, J.A. and L.-S. Fan. (2015). Process Development of Manganese-Based Oxygen Carriers for Oxidative Coupling of Methane in a Pressurized Chemical Looping System. Conference Proceedings presented at the 2015 American Institute of Chemical Engineers (AIChE) Spring Meeting and 11th Global Congress on Process Safety, Austin, Texas.

Fields of Study

Major Field: Chemical and Biomolecular Engineering

Table of Contents

Introduction

The opportunity of converting the world's most abundant hydrocarbon feedstock into the world's most important commodity chemical has attracted researchers to study the oxidative coupling of methane (OCM) to ethylene since the 1980s. Despite its availability, methane is highly stable relative to other hydrocarbons and thus is traditionally used as a fuel. The discovery of new reserves of shale gas in the United States has emphasized the value a direct conversion pathway for methane would add to the national and global economy (Armor, 2013). Pioneering work in upgrading methane to ethylene identified multiple metal oxides and oxygen delivery methods to execute this reaction (Keller & Bhasin, 1982). This idea is significant because it challenges steam cracking, the predominant pathway to ethylene via ethane or naphtha from crude oil. From a sustainability perspective, the steam cracking of hydrocarbon feedstocks to ethylene and its coproducts is the most energy intensive process in the petrochemical industry (Worrell, Phylipsan, Einstein, & Martin, 2000). Full-scale development of OCM provides an opportunity to lower the energy consumption of conventional ethylene-producing reactions. This is due to the exothermic heat of reaction in the oxidative coupling of methane (reactions (1) and (2)) which can be integrated into the process or used for electricity generation. Steam cracking is an endothermic reaction (reaction (3)), thus adding to the energy footprint of the process.

$2CH_4 + ½ O_2 \rightarrow C_2H_6 + H_2O$ $\Delta H° = -176.6$ kJ/mol (1)

$C_2H_6 + ½ O_2 \rightarrow C_2H_4 + H_2O$ $\Delta H° = -105.5$ kJ/mol (2)

$C_2H_6 \rightarrow C_2H_4 + H_2$ $\Delta H° = +137$ kJ/mol (3)

Despite the attractiveness of OCM, many barriers must be overcome before commercialization is achieved. These obstacles include high temperatures of reaction (700ºC - 800ºC), thermodynamic favorability of CO_2 formation, limitations on conversion and yield imposed by explosion limit of O_2 in feed, separation of ethylene, low selectivity at higher conversion (Farsi & Mansouri, 2016). Because of these complex parameters, the best route to commercialization has been debated in the OCM research community. The two main approaches include the cofeed method and the cyclic reduction-oxidation (redox) method. The cofeed method offers clear advantages, mainly operation at steady state conditions. Siluria arguably has been the most successful entity in scaling this endeavor. The Siluria technology operates at several hundred degrees lower than standard OCM reactors and cofeeds oxygen or air with the feedstock over a nanowire catalyst (Siluria Technologies, Inc., 2014). However, competing oxidation reactions of methane with molecular oxygen make combustion to carbon oxides an unavoidable side reaction. Keller and Bhasin identified a key advantage of the redox strategy, reporting higher selectivity results when using metal oxides to deliver oxygen to methane. These metal oxides are termed catalytic oxygen carriers (COCs), as they have the capability to hold one reactant while the other is fed. The redox mode also eliminates the need of an air separation unit, which is used to deliver a continuous stream of oxygen

to the reactant (Chung, Wang, Nadgouda, Baser, Sofranko, & Fan, 2016). Additionally, redox mode reduces the risk of operating within the flammability limits of methane and oxygen through the use of COCs. This study attempts to elucidate the structure-function relationships of COCs to provide insight into the prerequisites for successful OCM particle technology.

Literature reports redox modes using doped manganese oxides as COCs have produced the most promising yields in cyclic OCM operations (Xueping, Shuben, Jingzhu, Jingfang, & Dexin, 1992). These compounds are effective in abstracting molecular oxygen to create active sites for methane. The hydrogen is then stripped from the methane, forming hydroxide and methyl radicals on the COC surface (Lomonosov & Sinev, 2016). It is commonly accepted that ethane is formed by the combination of methyl radicals in the gas phase. Ethylene and C_{3+} hydrocarbons are similarly formed through a dehydrogenation pathway via subsequent reactions with the COC active sites. The marked increase in C_2 selectivity observed from doping metal oxides with Li^+ have been directly correlated to an increase in methyl radical formation (Hutchings & Woodhouse, 1989). Thermogravimetric analyses with various COCs have suggested the presence of multiple types of oxygen within the particle lattice. An Mg_6MnO_8 derivative studied by Chung et. al. exhibited two types of lattice oxygen that participated in the reaction with methane. One of these types of oxidants was more reactive yet less selective, and was termed loosely bound oxygen. The other type of oxidant exhibited slower reduction rates, and was termed the strongly bound oxygen. It was hypothesized in this study that the strongly bound oxygen was responsible for more selective oxidation

of the methane and was the rate limiting step in conversion. This behavior is seen in chemical-looping with oxygen uncoupling (CLOU) materials. CLOU materials are unique because they exhibit partial pressures of molecular oxygen at certain temperatures. This is reported as advantageous in rate-limited gasification reactions with solid oxides, as the reactant gas can interact with the released molecular oxygen without gasification (Azimi, Mattisson, Leiona, Rydén, & Lyngfelt, 2015). The transition between loosely and strongly bound oxygen is modeled by the transition between Mn oxidation states (Burch, Chalker, Squire, & Tsang, 1990). The COCs used in this study were doped and non-doped versions of Mg_6MnO_8, a particle that has three oxidation states: $Mn4^+$, $Mn3^+$, and $Mn2^+$. The most oxidized state is Mn^{4+}, and constitutes the loosely bound oxygen. The intermediate oxidation state is Mn^{3+}. This state constitutes the strongly bound oxygen, and has been attributed to activation of the C-H bond for methyl radical formation in the OCM reaction mechanism (Lee & Oyama, 1988). The fully reduced state is Mn^{2+}, which is not useful in further oxidation reactions until the COC is regenerated.

Mg_6MnO_8, henceforth referred to as MMO, and $Li_{0.2}Mg_{5.8}MnO_8$, henceforth referred to as Li-MMO, were used as the COCs in fixed bed and TGA experiments. This system was able to elucidate the effects of Li-doping, CLOU materials, and Mn oxidation states on COC function in an OCM process. More generally, MMO and Li-MMO were selected to identify nuanced oxygen delivery mechanisms in an attempt to explain selectivity and conversion trends seen in OCM redox experiments. These learnings on

structure-function relationships of COCs can be leveraged to clarify oxygen delivery strategies for other chemical looping applications.

Experimental

Catalytic Oxygen Carrier Preparation

The COCs used in this study include Mg_6MnO_8, henceforth referred to as MMO, and $Li_{0.2}Mg_{5.8}MnO_8$, henceforth referred to as Li-MMO. These particles were prepared in 20 gram batches via wet mixing. For the preparation of Li-MMO, stoichiometric amounts of LiOH (Sigma-Aldrich), MgO (Materion) and MnO_2 (Materion) were mixed with 20 mL of DI water. The resulting particle was calcined under steady air flow controlled with a mass flow controller (Alicat Scientific, Inc.). After calcination was complete, the COC was sieved to a particle diameter of 350 – 800 μm. The preparation for MMO was identical to the above procedure except for the addition of the LiOH powder.

Thermogravimetric Analysis (TGA)

TGA (Setaram Setsys Evolution TGA) was used to characterize COC oxygen content and regeneration over multiple redox cycles. A pair of TGA experiments was performed to elucidate the structure-function relationships of each COC that could be attributed to lattice oxygen. The first TGA experiment evaluated the strongly and loosely bound oxygen content of each COC by developing a reduction profile. A sample of approximately 25 mg was loaded onto a ceramic TGA crucible. Gas flow rate was maintained at 200 mL/minute with a mass flow controller (Alicat Scientific, Inc.). The temperature of the sample was then ramped to 850^{o}C at a rate of 20^{o}C per minute with a constant flow rate of air. To quantify loosely bound oxygen content, the sample was exposed to nitrogen for 14 - 15 hours. Subsequently, the sample was reduced by a gas

mixture of 10% methane balanced by nitrogen for 5 minutes to quantify strongly bound oxygen content. COC performance over multiple redox cycles was similarly evaluated in the second TGA test. After the desired temperature of 850^{o}C was achieved in the TGA, the COC was subjected to 15 redox cycles of a 5-minute reduction and 30-minute oxidation step, each followed by a 5-minute nitrogen purge. Gas flow rate was maintained at 200 mL/min during each step, and the reduction gas mixture consisted of 10% methane balanced by nitrogen.

Fixed Bed Experiments

Fixed bed experiments with the COCs were executed in the same apparatus as described in Chung, et. al. (Chung, Wang, Nadgouda, Baser, Sofranko, & Fan, 2016).The experiments were operated at 850^{o}C and 101 MPa under adiabatic conditions. The reactor bed was loaded with COC surrounded by alumina silica wool, and the COC volume was held constant for all experiments. A K type thermocouple (Omega) was inserted into the ceramic reactor during the fixed bed experiments to monitor the reaction temperature at the surface of the COC particle. Two types of redox experiments were performed to elucidate the varying effects of loosely and strongly bound COC oxygen on the product distribution. Cofeed experiments were attempted in order to compare the effects of oxygen delivery methods on the product distribution. However, a fair comparison between redox and cofeed modes was not possible without crossing the flammability limits of the reactant gases or fluidizing the fixed bed. This is discussed more in detail in the Results and Discussion.

Gas Product Analysis

Samples of gas products were manually bagged and analyzed via GC-MS analysis. The bagged samples were manually injected into a gas chromatograph (GC; Agilent 7890B) with a mass spectrometer (MS; Agilent 5977A) via a gas-tight syringe. The gases were equally split and separated on two different columns connected to two different detectors within the GC. The sample was separated for methane, nitrogen, carbon monoxide and carbon dioxide by a Carboxen 1006 PLOT capillary column and analyzed by a thermal conductivity detector (TCD). The sample was also separated for methane, ethylene, ethane and all hydrocarbons up to C_7 by a GS-Q Agilent J&W GC column and analyzed by a flame ionization detector (FID) and the MS.

Strongly Bound Versus Strongly and Loosely Bound Oxygen

The effects of strongly and loosely bound oxygen on product distribution were elucidated by a chemical looping approach. Due to the ability of the COC to extract molecular oxygen at the high reaction temperatures, oxidation of methane was enabled by cyclic reduction and regeneration of the COC. These redox cycles consisted of a 15 second reduction with methane and a 30 min oxidation with air. Both the reduction and oxidation steps were followed by a 10 min nitrogen purge, amounting to a 50 min and 15 sec total redox cycle time. Methane, air, and nitrogen flow rates were maintained at 200 mL/min to achieve a GHSV of 2400 hr^{-1}. Preparing the COC for the strongly bound oxygen experiments entailed removing all of the loosely bound surface oxygen at the $Mn4^{+}$ oxidation state. First, the COC was activated by exposing the particle to a series of consecutive redox cycles at reaction temperature. MMO and Li-MMO were activated

with 5 and 10 redox cycles, respectively. Subsequently, elimination of the loosely bound oxygen was achieved by exposing the COC bed to constant flow of nonreactive gas for 12 to 16 hours while maintaining a reactor temperature of 850^{o}C. After the loosely bound oxygen was reduced from the Mn^{4+} to the Mn^{3+} oxidation state, the redox cycle sequence was initialized. Gas samples were manually bagged within the first 5 to 10 sec and 10 to 15 sec windows of the reduction cycle. The beginning portion the reduction step was not analyzed because of a 5 sec gas residence time. The samples were injected into the GC-MS for product analysis. The strongly and loosely bound oxygen studies were similarly executed, which analyzed the effect of the Mn^{4+} oxidation state on product distribution. However, the COC in these experiments was not subjected to a 12 to 16 hour nitrogen purge to redude the loosely bound oxygen to the Mn^{3+} state. Rather, once the reactor reached the desired temperature the redox cycle sequence was initialized and allowed to operate for 6 to 10 complete cycles. Gas samples were similarly collected and analyzed, and the data from the final reduction cycle was reported. Selectivity, conversion, and yield were the key performance indicators used for each experiment. The calculations for these figures are shown in Equations E1 – E4 below.

$$Selectivity\ \% = \frac{[Carbon]_{C_2 and\ C_{2+}}}{[Carbon]_{C_2,\ C_{2+}, and\ CO_2}} * 100\% \quad \text{(E1)}$$

$$Conversion\ \% = \frac{[Carbon]_{C_2,\ C_{2+}, and\ CO_2}}{[Carbon]_{C_2,\ C_{2+},\ \ CO_2, and\ CH_4}} * 100\% \quad \text{(E2)}$$

$$Yield\ \% = \frac{Selectivity\ \% * Conversion\ \%}{100} \quad \text{(E3)}$$

$$Product\ Selectivity\ \% = \frac{[Product]}{[Carbon]_{C_2,\ C_{2+}, and\ CO_2}} * 100\% \quad \text{(E4)}$$

Results and Discussion

TGA Experiment Results

The TGA experiments were critical in characterizing the COC as well as validating the results from the fixed bed experiments. Figures RD-1 and RD-2 show the TGA results for the MMO and Li-MMO COC when subjected to 15 consecutive redox cycles. The initiation of the oxidation step in the first full cycle is indicated by a green triangle, and the initiation of the reduction step in the first full cycle is similarly indicated by a red circle. The start of each nitrogen purge step is indicated by a purple square. The initial gain in mass is due to the molecular oxygen binding to the COC during the initial temperature ramp under 200 mL/min of air.

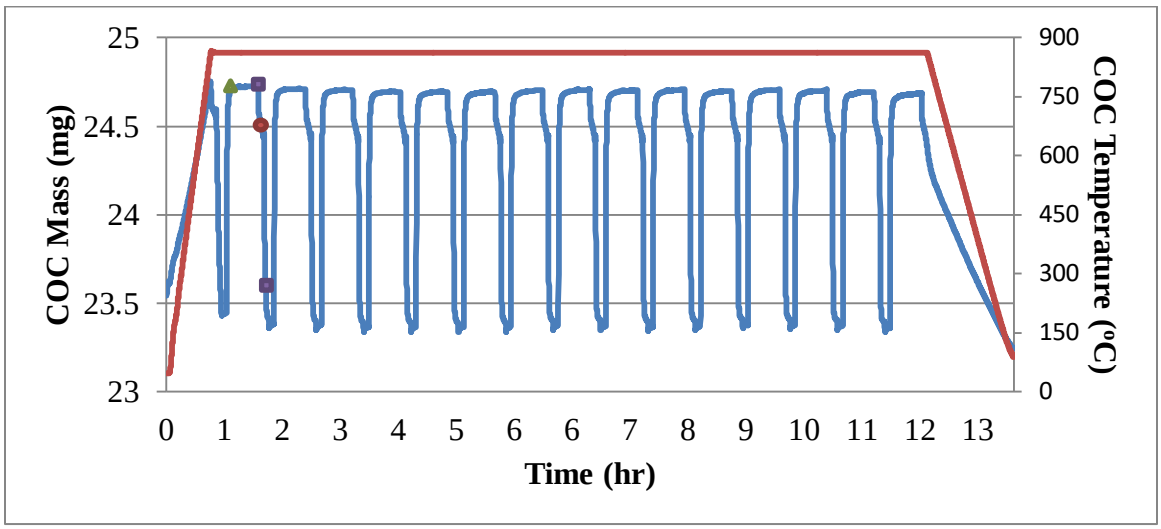

Figure RD-1: MMO TGA results for 15 redox cycles at 850°C.

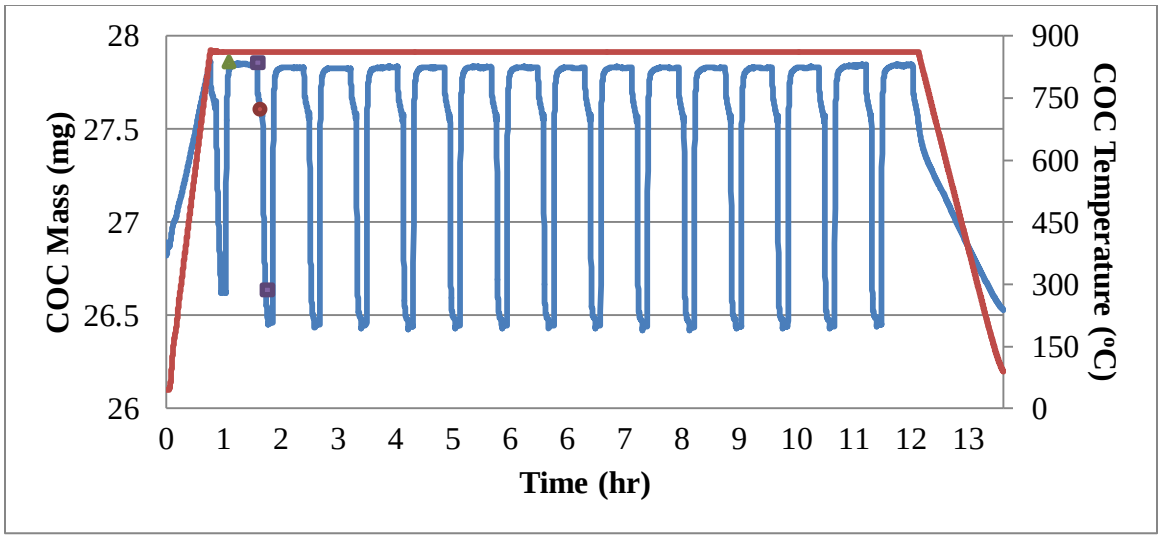

Figure RD-2: Li-MMO TGA results for 15 redox cycles at 850°C.

The MMO maximum particle mass after oxidation did not change by more than 0.02% throughout the TGA regeneration study. Furthermore, the MMO minimum particle mass after reduction did not change by more than 0.04% throughout the TGA study shown in Figure RD-2. Both the Li-MMO maximum and minimum particle mass only changed by about 0.01% throughout the course of the 15 redox cycles. Therefore, the MMO and Li-MMO particles were assumed to maintain their activity after multiple redox cycles, a quality which is regarded as a prerequisite to develop a commercially viable COC (Chung et. al.). This data informed the data collection strategy as well as validated the repeatability of the fixed bed experiments.

Calculating the difference in COC mass between the oxidation step and the reduction step revealed the percent mass constituted by oxygen consumed in a single reduction step. The average oxygen consumed by MMO and Li-MMO in a single reduction step was 5.25% ± 0.10% and 4.88% ± 0.02% of the total COC mass,

respectively. The data show that the reduction rate of the MMO was 20.1 mg/hr when both Mn^{4+} and Mn^{3+} states were present in the COC. This was 42% faster than the Li-MMO counterpart. Addition of Li as a dopant to MgO has been shown decrease the activation rate of the methane, thus increasing the C_2 selectivity in the product distribution (Ito & Lunsford, 1985). Increases in C_2 selectivity coupled by decreases in methane conversion have been an inherent barrier to the commercialization of OCM processes (Sofranko, Leonard, Jones, Gaffney, & Withers, 1988). Furthermore, Sofranko et. al. proposed the presence of excess molecular oxygen in cofeed modes of operation was responsible for a 5-10% loss in selectivity when compared to cyclic reaction modes. These conclusions have been extended to the results discussed above in which the Li-doped MMO has a lower oxygen content than the non-doped MMO. It is therefore hypothesized that the reported increase in selectivity for the Li-doped COC is due to the lowered rate of oxidation inspired by the $[Li^+ OH^-]$ centers.

The work of Sofranko et. al. further proposed the difference in product distribution between cofeed and cyclic oxidation modes was suspected to be due to the dependence of reaction mechanism on oxidant species, e.g. molecular or lattice oxygen. This discussion has been continued with this study, as the lattice oxygen itself was hypothesized to have varying contributions to product selectivity and methane conversion. More accessible, loosely bound oxygen on the surface of the COC was predicted to produce a lower C_2 selectivity and higher methane conversion when compared to strongly bound lattice oxygen within the same COC particle. The relative abundance of strongly and loosely bound lattice oxygen within MMO and Li-MMO was

quantified via reduction profile TGA experiments. Exposing fully oxidized COC particles to a steady nitrogen purge for about 13 hours revealed loosely bound oxygen content for MMO and Li-MMO to be 3.3% and 3.1% respectively. Subsequent reduction with 10% methane balanced by nitrogen revealed strongly bound oxygen content for MMO and Li-MMO to be 2.6% and 1.7%, respectively. The TGA reduction profiles for both COCs are shown in Figures RD-3 and RD-4. Table RD-1 summarizes the key data from these experiments.

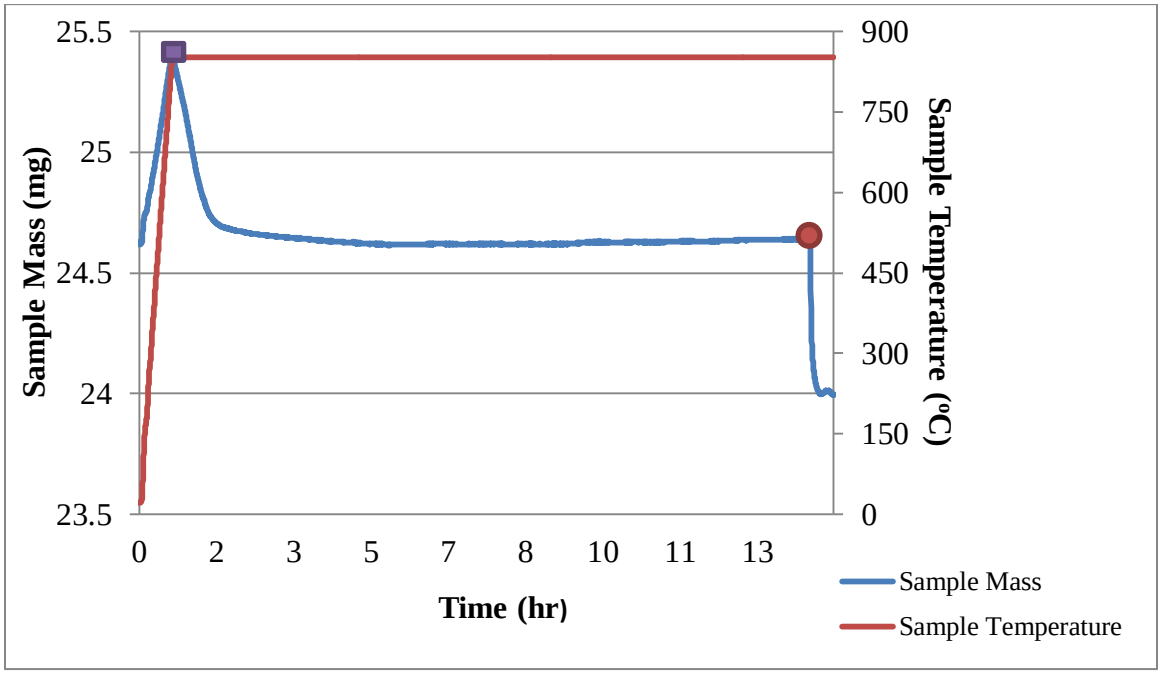

Figure RD-3: Reduction profile for MMO at 850°C. The initiation of the nitrogen purge and the reduction gas steps are indicated by the purple square and red circle, respectively.

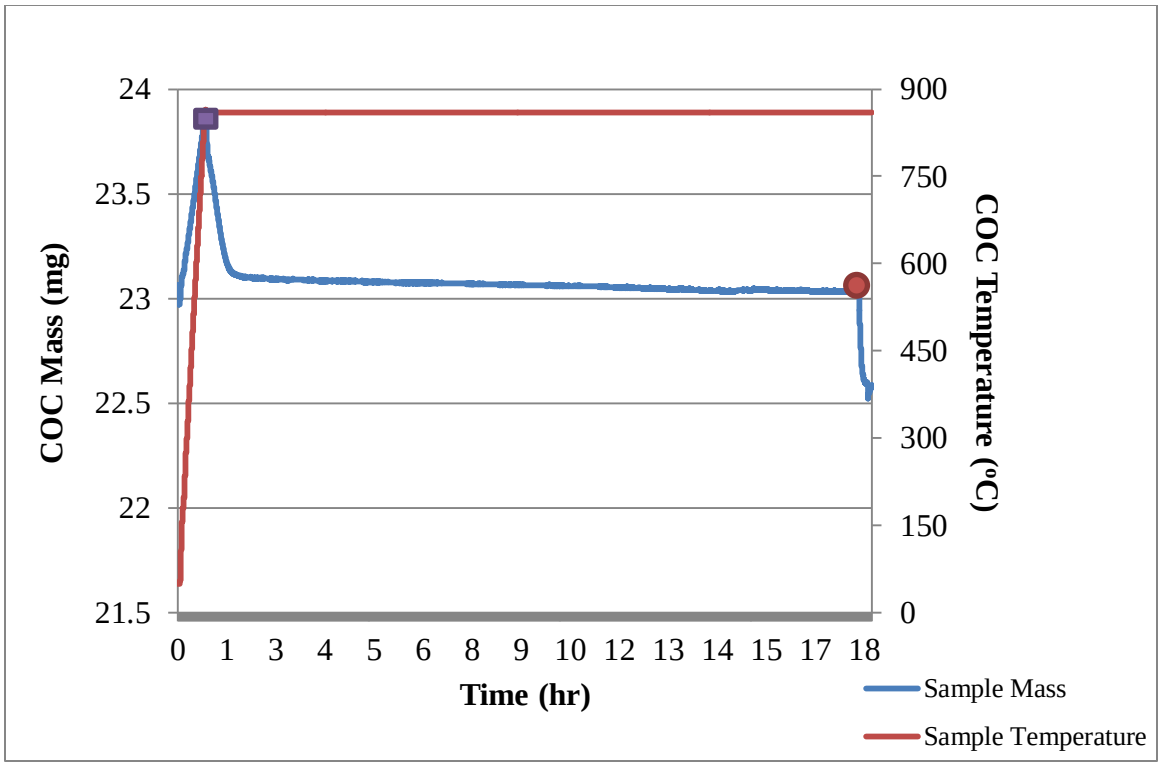

Figure RD-4: Reduction profile for Li-MMO at 850°C. The initiation of the nitrogen purge and the reduction gas steps are indicated by the purple square and red circle, respectively.

Table RD-1: Data summary for TGA experiments on MMO and Li-MMO at 850°C.

COC	% Mass Loosely Bound Oxygen (w/w)	% Mass Strongly Bound Oxygen (w/w)	Reduction Rate of Strongly and Loosely Bound Oxygen (mg/hr)	Reduction Rate of Strongly Bound Oxygen (mg/hr)
MMO	3.1%	2.7%	20.1	6.6
Li-MMO	3.3%	1.9%	14.2	4.2

Table RD-1 illustrates how the lithium dopant decreases reduction rate of both the manganese oxidation states, influencing MMO to function more selectively in oxidizing methane to C_{2+} products. It is critical to note the rate of reduction of the strongly bound oxygen was considerably slower than the rate of reduction of both the strongly and loosely bound oxygen. Reduction rate is heavily discussed in literature evaluating the mechanisms of OCM. Typically, slower reduction rates lead to higher selectivity and lower conversion. Therefore, it was predicted that the strongly bound oxygen from the Mn^{3+} oxidation state would perform accordingly in the fixed bed experiments.

Fixed Bed Experiments

Previous studies have shown that both the loosely and strongly bound oxygen react simultaneously in a complex reaction mechanism (Chung, Wang, Nadgouda, Baser, Sofranko, & Fan, 2016). Therefore, it was impractical to compare loosely bound oxygen with strongly bound oxygen on the COCs studied in the fixed bed experiments. However, the effect of loosely bound oxygen on product distribution was elucidated by eliminating all loosely bound surface oxygen on the COC lattice. This was done by reducing the COCs under nitrogen from the Mn^{4+} oxidation state to the Mn^{3+} state. The resulting particle only contained strongly bound lattice oxygen. The effects of the loosely bound oxygen on C_2 selectivity, methane conversion, and production distribution were identified by comparing fixed bed results of strongly and loosely bound lattice oxygen with the strongly bound lattice oxygen. Figures RD-5 and RD-6 show the selectivity and conversion resulting from the strongly bound oxygen fixed bed experiments.

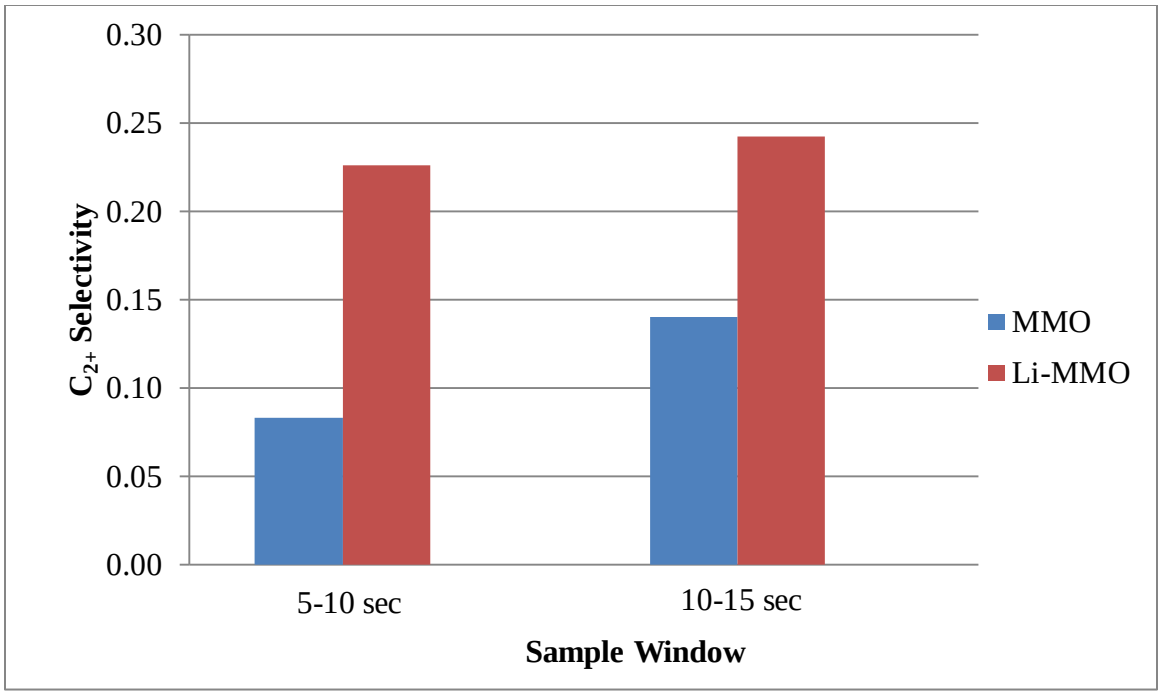

Figure RD-5: C_{2+} selectivity values for strongly bound oxygen as the oxidant at 2400^{-1} GHSV and 850°C.

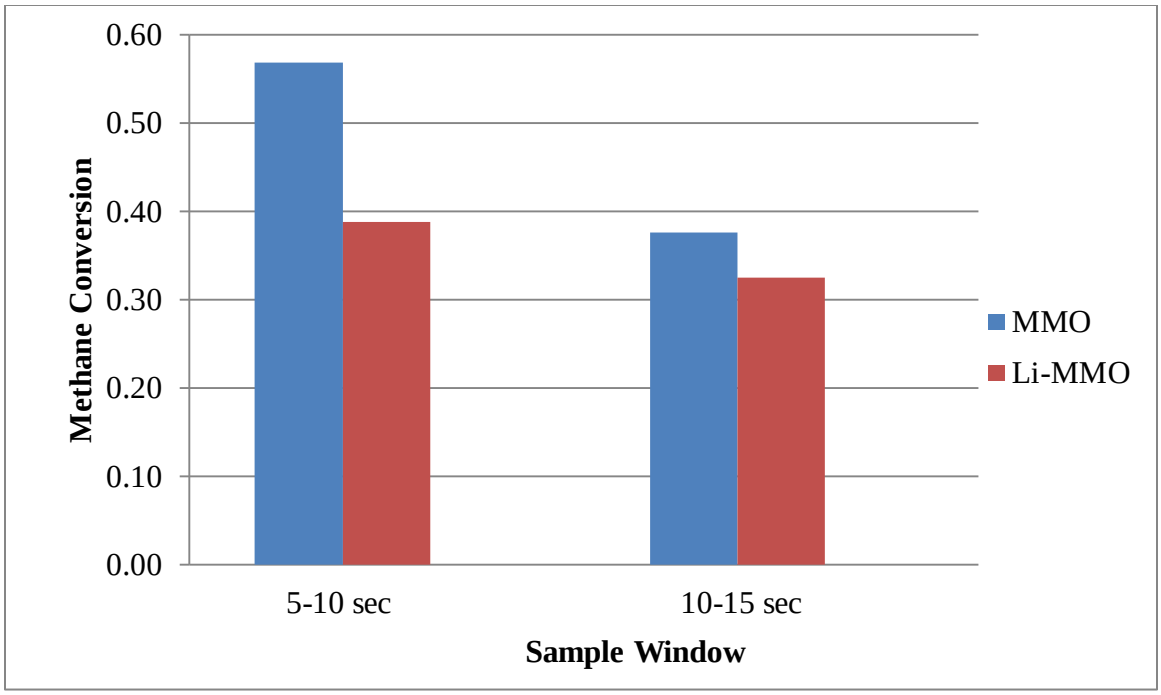

Figure RD-6: Methane conversion values for strongly bound oxygen as the oxidant at 2400^{-1} GHSV and 850°C.

In comparing MMO and Li-MMO, the C_{2+} selectivity for the Li-MMO was higher while the conversion for the non-doped MMO was higher. These fixed results corroborate with the TGA results discussed above. MMO was suspected to have a higher conversion than Li-MMO due to its relatively higher rate of methane reduction. Conversely, Li-MMO performed as hypothesized due to its relatively slower kinetics. The yield and product distribution from the COC strongly bound oxygen are shown in Tables A-1 through A-4 in Appendix A: Product Distribution Tables for Fixed Bed Experiments. Small quantities (less than 1% of the product distribution) of acetylene, propane, propylene, unidentified C_3 products, and unidentified C_4 products were also

generated by both COCs studied, more markedly by the Li-MMO. The generation of propane, propylene, and other C_{3+} hydrocarbons has been reported in other OCM studies, however ethane and ethylene have typically been the primary products (Sinev, Fattakhova, Lomonosov, & Gordienko, 2009). The presence of C_{3+} hydrocarbons has been explained by kinetic modeling of the reaction of free methyl radicals with ethylene and ethane (Lomonosov & Sinev, 2016).

The loosely and strongly bound lattice oxygen affected the product distribution of methane oxidation as was predicted by the discussion around the TGA results. The additional lattice oxygen provided to the reactant gas resulted in increased methane conversion. Each fixed bed test performed with loosely and strongly bound oxygen as the oxidant showed an increase in methane conversion and a subsequent decrease in C_{2+} selectivity when compared to its counterpart in which only strongly bound oxygen was available. Figures RD-7 and RD-8 show the selectivity and conversion resulting from the strongly bound oxygen fixed bed experiments.

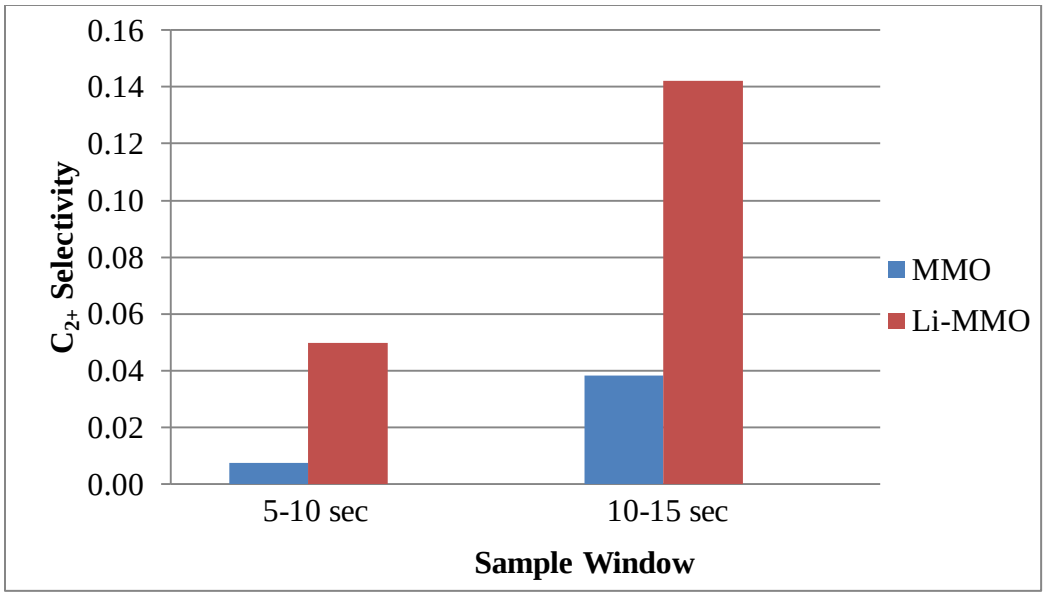

Figure RD-7: C_{2+} selectivity results for loosely and strongly bound oxygen as the oxidant at 2400^{-1} GHSV and 850°C.

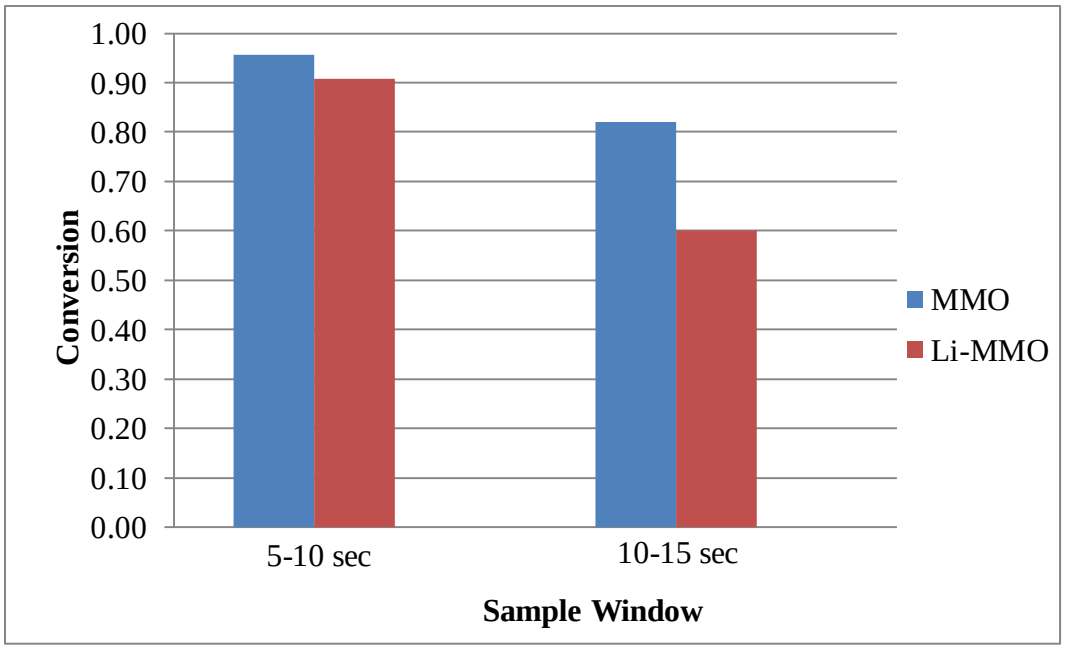

Figure RD-8: Methane results for loosely and strongly bound oxygen as the oxidant at 2400^{-1} GHSV and 850°C.

Similar to the results from the strongly bound oxygen fixed bed experiments, the MMO outperformed the Li-MMO in conversion while the opposite was observed for selectivity. This further substantiates the claim that the location of the lattice oxygen species has an effect on the product distribution in the oxidative coupling of methane. The product distributions from the loosely and strongly bound oxygen fixed bed experiments are shown in Tables A5-A8. Furthermore, the fixed bed experiment yields reported in Tables A1-A8 suggest Li-MMO was overall more effective than its non-doped counterpart in upgrading methane to higher value feedstocks, as has been reported with Li/MgO systems (Hutchings, Scurrell, & Woodhouse, 1989).

It was observed that product distribution was also affected by sampling time after reduction. Gas product samples taken within the first five seconds of the reduction step varied in composition and methane conversion with product samples taken within the first ten seconds of the reduction step. This observation is clear from the data displayed in Figures RD-1 through RD-4. All the data sets showed a decrease in methane conversion as reduction time progressed while displaying the opposite trend for conversion. Chung et. al. also observed this in fixed bed redox experiment with a proprietary COC described as doped Mg_6MnO_8. This dynamic COC behavior was explained by the consumption of the accessible loosely bound oxygen at a more rapid rate than the strongly bound oxygen species. The effect of reduction time on product distribution further supported the hypothesis that different types of oxygen species on the COC lattice fulfill varying roles in the oxidative coupling of methane. As the loosely bound oxygen reserves are depleted,

the COC performance shifts, indicating a change in oxidant regime. This is also described as the gradual reduction of Mn^{4+} to the Mn^{3+} state.

A series of cofeed experiments were attempted in the fixed bed to complete the study on varying catalytic oxygen delivery strategies for methane upgrading. In order to fairly compare the results from cofeed and redox, an experiment was designed to ensure the same amount of oxygen was delivered in both reaction modes. The mass of loosely bound oxygen on the COC was calculated from the TGA reduction profile. An equivalent volume of molecular oxygen was calculated for the purpose of cofeeding the oxidant with the reducing gas over the COC during the 15 second reduction step. This would essentially replace the loosely bound oxygen content of the COC with molecular oxygen, allowing for a robust comparison between cofeed and redox modes of operation. However, these efforts were unsuccessful because oxygen flow rate and composition posed risks of surpassing both the minimum fluidization velocity and the lower explosion limits of oxygen in methane. Indeed, the lower explosion limit of oxygen has been indicated as a barrier to the commercialization of OCM processes (Farsi & Mansouri, 2016). Efforts were made to dilute the cofeed reactant gas stream with nitrogen and thus eliminate flammability risks. However, after these dilution calculations were performed, the independent variables in the cofeed experiments were confounded. Figure 1 includes the flammability triangle for methane with the points shown where cofeed experiments would have been executed. The black line indicates possible cofeed reactant gas compositions to maintain the same ratio of oxygen to methane that was available in loosely bound oxygen redox experiments with Mn^{3+} as the starting COC oxidation state.

The red circles represent feed gas compositions on the black line with twofold, fourfold, and eightfold nitrogen dilutions. In order to deliver the same methane and oxygen ratios as originally intended, the feed gases would have required an eightfold dilution in nitrogen.

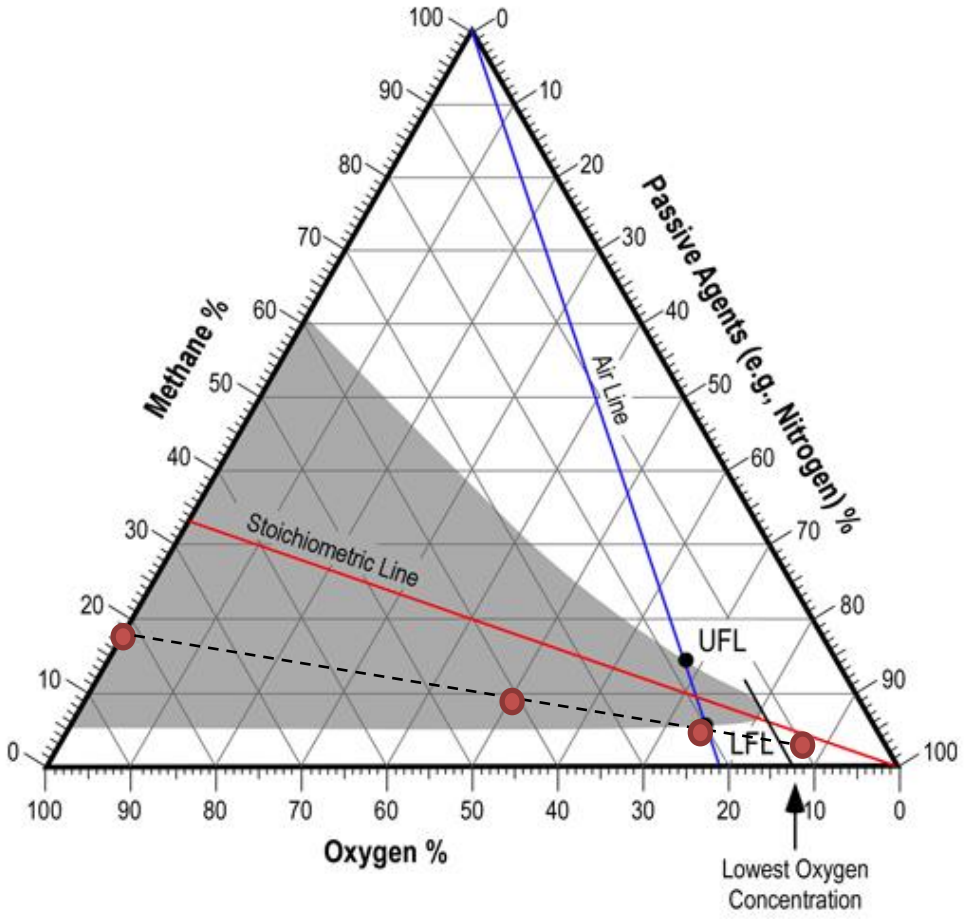

Figure RD-9: Flammability triangle for methane. The cofeed reactant gas composition required to match the oxygen delivered in a redox experiment is indicated by the red circles.

Due to the necessity for dilution with passive agents imposed by the flammability limits, robust comparisons of cofeed and redox modes of operation could no longer be

made. At the very least, this emphasizes the difficulty in commercialization imposed by the parameters of the OCM process. Furthermore, this illustrates an advantage of redox modes over cofeed modes, as cyclic operation eliminates the risk of mixing the oxygen source with the reducing gas. Even though the experiment was not completed, it was predicted that cofeeding oxygen would positively impact methane conversion while negatively influencing product selectivity towards ethane and ethylene. Molecular oxygen is even more accessible and non-selective than the loosely bound lattice oxygen. Indeed molecular oxygen has been known to participate in competitive reactions in which the OCM products and intermediates are combusted to carbon dioxide (Keller & Bhasin, 1982). Cofeed mode experiments were therefore expected to influence the reaction accordingly, not adding any new value to the OCM discussion.

Conclusion

The presence of different types of lattice oxygen is a known attribute of OCM COCs as well as other heterogeneous oxidant systems. The hypothesis that the Mn^{3+} and the Mn^{4+} oxidation states within MMO and Li-MMO both function differently in oxygen delivery is strongly supported by this work. More specifically, it was proposed that the loosely bound oxygen from the Mn^{3+} state contributed to relatively non-selective methane conversion while the strongly bound oxygen from the Mn^{4+} state was governed by slower yet more selective reaction kinetics. These claims were supported by the findings in TGA and fixed bed experiments with the COCs. The TGA data supported the assertion that loosely bound oxygen contributing more to non-selective conversion. Having faster reduction rate in the presence of methane, MMO was predicted to outperform Li-MMO in methane conversion and underperform in C_{2+} selectivity. Oxygen content did not have as large a role in COC behavior as expected. The fixed bed results complemented the TGA data and showed that each product distribution mediated by MMO a higher conversion than the product distribution from Li-MMO. Conversely, Li-MMO produced hydrocarbon suites with higher C_{2+} selectivity in every test when compared to MMO. Finally, the effect of sample time on product distribution further illustrates the contrasting roles of loosely and strongly bound lattice oxygen. As loosely bound oxygen was consumed, the product distribution responded by showing consistent trends of decreases in methane conversion and increases in C_{2+} selectivity. Finally, fixed bed experiments aimed to isolate the effects of loosely and strongly bound oxygen unanimously showed product distribution patterns consistent with expected trends. These

findings provide an opportunity to explore future COCs for optimizing product distribution in the oxidative coupling of methane.

References

Armor, J. N. (2013). Emerging importance of shale gas to both. *Journal of Energy Chemistry*, 21-26.

Azimi, G., Mattisson, T., Leiona, H., Rydén, M., & Lyngfelt, A. (2015). Comprehensive study of Mn–Fe–Al oxygen-carriers for chemical-looping with oxygen uncoupling (CLOU). *International Journal of Greenhouse Gas Control*, 12-24.

Burch, R., Chalker, S., Squire, G. D., & Tsang, S. C. (1990). Oxidative Coupling of Methane over Manganese Oxide Catalysts. *Journal of the Chemical Society*, 1607-1614.

Chung, E. Y., Wang, W. K., Nadgouda, S. G., Baser, D. S., Sofranko, J. A., & Fan, L.-S. (2016). Catalytic Oxygen Carriers and Process Systems for Oxidative Coupling of Methane Using the Chemical Looping Technology. *The Royal Society of Chemistry*.

Farsi, A., & Mansouri, S. (2016). Influence of nanocatalyst on oxidative coupling, steam and dry reforming of methane: A short review. *Arabian Journal of Chemistry*, S28-S34.

Hutchings, G. J., & Woodhouse, J. R. (1989). Partial Oxidation of Methane over Oxide Catalysts. *Journal of the Chemical Society*, 2507-2523.

Hutchings, G., Scurrell, M., & Woodhouse, J. (1989). Oxidative Coupling of Methane using Oxide Catalysts . *Chemical Society Reviews*, 251-283.

Ito, T., & Lunsford, J. (1985). Synthesis of ethylene and ethane by partial oxidation of methane over lithium-doped magnesium oxide. *Nature*, 721-722.

Keller, & Bhasin. (1982). Synthesis of Ethylene via Oxidative Coupling of Methane: I. Determination of Active Catalysts. *Journal of Catalysis*, 9-19.

Lee, J., & Oyama, S. (1988). Oxidative Coupling of Methane to Higher Hydrocarbons. *Catalysis Reviews. Science and Engineering.*, 249-280.

Lomonosov, K., & Sinev, M. Y. (2016). Oxidative Coupling of Methane: Mechanism and Kinetics. *Kinetics and Catalysis*, 647-676.

Siluria Technologies, Inc. (2014). Oxidative Coupling of Methane. San Francisco, CA.

Sinev, M. Y., Fattakhova, Z. T., Lomonosov, V., & Gordienko, Y. A. (2009). Kinetics of oxidative coupling of methane: bridging the gap between comprehension and description. *Journal of Natural Gas Chemistry*, 273-287.

Sofranko, J., Leonard, J., Jones, C., Gaffney, A., & Withers, H. (1988). CATALYTIC OXIDATIVE COUPLING OF METHANE OVER SODIUM-PROMOTED Mn/SiO, . *Catalysis Today*, 127-135.

Worrell, E., Phylipsan, D., Einstein, D., & Martin, N. (2000). *Energy Use and Energy Instensity of the U.S. Chemical Industry.* San Francisco: Lawrence Berkeley National Laboratory.

Xueping, F., Shuben, L., Jingzhu, L., Jingfang, G., & Dexin, Y. (1992). Preparation and Characterization of Catalyst for Oxidative Coupling of Methane. *Journal of Molecular Catalysis*, 2.

Appendix A: Product Distribution Tables for Fixed Bed Experiments

Table A-1: Product distribution for MMO with strongly bound oxygen as the oxidant within the 5-10 second sampling window.

	Selectivity (%)
Ethane	3.84
Ethylene	4.31
Propane	0.10
Propylene	0.05
Carbon Dioxide	91.71
Overall Yield (%)	4.71

Table A-2: Product distribution for MMO with strongly bound oxygen as the oxidant within the 10-15 second sampling window.

	Selectivity (%)
Ethane	6.61
Ethylene	7.02
Propane	0.20
Propylene	0.08
Unidentified C3	0.03
Unidentified C4	0.05
Carbon Dioxide	86.01
Overall Yield (%)	5.26

Table A-3: Product distribution for Li-MMO with strongly bound oxygen as the oxidant within the 5-10 second sampling window.

	Selectivity (%)
Ethane	9.08
Ethylene	11.73
Acetylene	0.70
Propane	0.58
Propylene	0.10
Unidentified C3	0.43
Carbon Dioxide	77.38
Overall Yield (%)	8.76

Table A-4: Product distribution for Li-MMO with strongly bound oxygen as the oxidant within the 10-15 second sampling window.

	Selectivity (%)
Ethane	10.02
Ethylene	12.49
Acetylene	0.44
Propane	0.72
Propylene	0.57
Carbon Monoxide	2.78
Carbon Dioxide	72.99
Overall Yield (%)	7.86

Table A-5: Product distribution for MMO with strongly and loosely bound oxygen as the oxidant within the 5-10 second sampling window.

	Selectivity (%)
Ethane	2.74
Ethylene	11.07
Propane	0.16
Carbon Dioxide	86.03
Overall Yield (%)	0.70

Table A-6: Product distribution for MMO with strongly and loosely bound oxygen as the oxidant within the 10-15 second sampling window.

	Selectivity (%)
Ethane	0.94
Ethylene	2.78
Propane	0.06
Propylene	0.02
Unidentified C3	0.01
Carbon Dioxide	96.18
Overall Yield (%)	3.13

Table A-7: Product distribution for Li-MMO with strongly and loosely bound oxygen as the oxidant within the 5-10 second sampling window.

	Selectivity (%)
Ethane	0.85
Ethylene	3.63
Acetylene	0.21
Propane	0.16
Propylene	0.13
Carbon Dioxide	95.02
Overall Yield (%)	4.52

Table A-8: Product distribution for Li-MMO with strongly and loosely bound oxygen as the oxidant within the 10-15 second sampling window.

	Selectivity (%)
Ethane	3.50
Ethylene	9.85
Acetylene	0.25
Propane	0.50
Propylene	0.12
Carbon monoxide	1.09
Carbon dioxide	84.69
Overall Yield (%)	8.53